Electrical coupling and release of K^+ from endothelial cells co-mediate ACh-induced smooth muscle hyperpolarization in guinea-pig inner ear artery

Zhi-Gen Jiang[1], Alfred L. Nuttall[1], Hui Zhao[1,2], Chun-Fu Dai[1,2], Bing-Cai Guan[1], Jun-Qiang Si[1,3] and Yu-Qin Yang[1]

[1]*Oregon Hearing Research Center, Oregon Health and Science University, Portland, OR 97239, USA*
[2]*Department of Otolaryngology, Eye Ear Nose and Throat Hospital, Fudan University, Shanghai, PR China*
[3]*Department of Physiology, Shihezi University Medical College, Xinjiang, PR China*

The physiological basis of ACh-elicited hyperpolarization in guinea-pig *in vitro* cochlear spiral modiolar artery (SMA) was investigated by intracellular recording combined with dye labelling of recorded cells and immunocytochemistry. We found the following. (1) The ACh-hyperpolarization was prominent only in cells that had a low resting potential (less negative than −60 mV). ACh-hyperpolarization was reversibly blocked by 4-DAMP, charybdotoxin or BAPTA-AM, but not by N^{ω}-nitro-L-arginine methyl ester, glipizide, indomethacin or 17-octadecynoic acid. (2) Ba^{2+} (100 μM) and ouabain (1 μM) each attenuated ACh-hyperpolarization by ∼30% in smooth muscle cells (SMCs) but had only slight or no inhibition in endothelial cells (ECs). A combination of Ba^{2+} and 18β-glycyrrhetinic acid near completely blocked the ACh-hyperpolarization in SMCs. (3) High K^+ (10 mM) induced a smaller hyperpolarization in ECs than in SMCs, with an amplitude ratio of 0.49 : 1. Ba^{2+} blocked the K^+-induced hyperpolarization by ∼85% in both cell types, whereas ouabain inhibited K^+-hyperpolarization differently in SMCs (19%) and ECs (35%) and increased input resistance. 18β-Glycyrrhetinic acid blocked the high K^+-hyperpolarization in ECs only. (4) Weak myoendothelial dye coupling was detected by confocal microscopy in cells recorded with a propidium iodide-containing electrode for longer than 30 min. A sparse plexus of choline acetyltransferase-immunoreactive (ChAT) fibres was observed around the SMA and its up-stream arteries. (5) Evoked excitatory junction potentials (EJP) were partially blocked by 4-DAMP in half of the cells tested. We conclude that ACh-induced hyperpolarization originates from ECs via activation of Ca^{2+}-activated potassium channels, and is independent of the release of NO, cyclo-oxygenase or cytochrome P450 products. ACh-induced hyperpolarization in smooth muscle cells involves two mechanisms: (a) electrical spread of the hyperpolarization from the endothelium, and (b) activation of inward rectifier K^+ channels (K_{ir}) and Na^+–K^+ pump current by elevated interstitial K^+ released from the endothelial cells, these being responsible for about 60% and 40% of the hyperpolarization, respectively. The role ratio of K_{ir} and pump current activation is at 8 : 1 or less.

(Resubmitted 9 December 2004; accepted after revision 21 February 2005; first published online 24 February 2005)
Corresponding author Z.-G. Jiang: Oregon Hearing Research Center, NRC04, Oregon Health & Science University, Portland, OR 97239, USA. Email: jiangz@ohsu.edu

Acetylcholine (ACh) is an intrinsic potent vasodilator in many vascular beds (Suga & Snow, 1969; Inoue & Kannan, 1988; Neild *et al.* 1990; Miao & Lee, 1991; Toda *et al.* 1997; Welsh & Segal, 1997). Fine fibres with varicose-like structures immunoreactive to choline acetyltransferase (ChAT) were observed in rat and cat brain arteries (Miao & Lee, 1991). ACh or its mimics dilate cochlear blood vessels and muscarinic antagonists reduce cochlear blood flow (Suga & Snow, 1969), suggesting a role of cholinergic control over the inner-ear circulation. Moreover, strong evidence suggests that vascular disturbances have been implicated in hearing losses of loud sound-induced trauma, ageing, Meniere's disease, drug ototoxicity and some forms of sudden deafness (Hultcrantz, 1988; Schuknecht & Gacek, 1993; Nuttall, 1999). The cellular and subcellular physiology of cholinergic regulation of inner

 DOI: 10.1113/jphysiol.2004.080960

ear vasculature may therefore have clinical relevance, but remain poorly investigated.

It is generally believed that ACh stimulates the endothelial cells (ECs) and releases an endothelium-derived hyperpolarizing factor (EDHF) that causes relaxation of the vascular smooth muscle cells (SMCs) (Feletou & Vanhoutte, 1999). The nature of ACh-released EDHF is complex and remains controversial among the reports (Faraci & Heistad, 1998; Feletou & Vanhoutte, 1999; Busse *et al.* 2002). ACh-induced EDHFs have been identified as K^+, nitric oxide (NO), prostaglandins, the cytochrome P450 products epoxyeicosatrienoic acids (EETs), and myoendothelial electrical coupling in vessel preparations from different organs and/or different animal species. For instance, possible involvement of the Na^+–K^+ pump in the ACh-induced hyperpolarization was first demonstrated by (Feletou & Vanhoutte, 1988) in the canine coronary artery. However, ACh-produced hyperpolarization was reportedly not affected by ouabain in the same preparation (Chen *et al.* 1989) and in rabbit ear artery (Suzuki, 1988). Later, Edwards *et al.* (1998; 1999*b*) showed that, in rat hepatic artery, ACh activates Ca^{2+}-activated K^+ channels (K_{Ca}) in ECs and thus raises the K^+ concentration in the myoendothelial space. The elevated K^+ concentration in turn hyperpolarizes the SMCs by activating Na^+–K^+-pump current and inward rectifier potassium channels (K_{ir}). Many other laboratories found evidence that failed to support such an EDHF pathway in various arteries, e.g. in guinea-pig carotid and coronary (Quignard *et al.* 1999), human subcutaneous (McIntyre *et al.* 2001), and rat mesenteric (Doughty *et al.* 2000; Lacy *et al.* 2000) and renal (Jiang & Dusting, 2001) arteries. Furthermore, strong evidence indicates that ACh induces hyperpolarization only in endothelial cells (ECs), and the electrical coupling between the endothelial and muscle layers is the *sole* mechanism responsible for the ACh-induced hyperpolarization in the SMCs in guinea-pig mesenteric arterioles (Imaeda *et al.* 2000; Yamamoto *et al.* 2001). One more example, Weidelt *et al.* (1997) reported that the ionic mechanism underlying the ACh-induced hyperpolarization in SMCs of rat mesenteric arteries has been attributed to activation of ATP-sensitive K^+ channels (K_{ATP}) and K_{Ca}, *solely* via release of NO from the endothelium, but mechanisms other than NO production were demonstrated later in the same artery (Edwards *et al.* 1999*a*).

We recently demonstrated that cells in the isolated cochlear spiral modiolar artery (SMA) of the guinea-pig have unique membrane properties (Jiang *et al.* 2001*a*; Zhao *et al.* 2002). Both smooth muscle and endothelial cells of the SMA exhibit bi-stable membrane resting potentials (RP), i.e. resting near −40 or −75 mV, termed low and high RP, respectively. The two distinct levels of RP are set mainly by all-or-none-like activation of K_{ir}. Relatively weak and heterogeneous electrical coupling exists among the SMCs, among the ECs and between these two types of cells. In the preliminary study, we found that ACh induced robust hyperpolarization only in the low RP cells whereas ACh elicited a depolarization in high RP cells, and the hyperpolarization in the SMCs, not in the ECs, was suppressed by a gap junction blocker by 84% (Jiang *et al.* 2001*a*,*b*), suggesting that an electrical coupling transmits the hyperpolarization from the EC to the SMC. Since elevated K^+ evokes a robust hyperpolarization that is not blocked by the gap junction blocker in the SMCs (Jiang *et al.* 2001*a*; Zhao *et al.* 2002), we thus hypothesize that ACh may cause a K^+ release from ECs which also contributes to the ACh-hyperpolarization in the SMCs. In this study, we tested this hypothesis and quantitatively identified a co-mediation mechanism of the ACh-induced EDHF. Preliminary data were reported as meeting abstracts (Jiang *et al.* 2001*b*, 2003, 2004).

Methods

Animals and spiral modiolar artery preparation

Guinea-pigs (250–500 g) were anaesthetized and then killed by exsanguination. The anaesthesia was accomplished by intramuscular injection of an anaesthetics mixture (1 ml kg^{-1}) of ketamine (500 mg), xylazine (20 mg) and acepromazine (10 mg) in 8.5 ml H_2O. Both bullae were rapidly removed and transferred to a Petri dish filled with a physiological solution (Krebs) composed of (mM): NaCl 125, KCl 5, $CaCl_2$ 1.6, $MgCl_2$ 1.2, NaH_2PO_4 1.2, $NaHCO_3$ 18, glucose 8.2, and saturated with 95% O_2 and 5% CO_2 at 35°C (pH 7.4). The spiral modiolar artery (SMA) was dissected out from the cochlea under a dissecting microscope. The vascular preparation was incubated for 0.5 h in the physiological solution and then transferred to a recording bath. A 2–5 mm long segment of the SMA was cleaned free of spongy connective tissues and pinned with minimum stretch to the silicone rubber layer (Sylgard 184, Dow Corning) in the bottom of an organ bath (volume 0.5 ml) and continuously superfused with a 35°C Krebs solution. When needed, a high potassium Krebs solution was made by additional KCl and accordingly reduced NaCl. The procedures were approved by the Institutional Animal Care and Use Committee of Oregon Health and Science University.

Intracellular recording

Intracellular recordings were made from a segment of the SMA (40–80 μm in outer diameter) in the basal and the second turn of the cochlea as previously described (Jiang *et al.* 1999, 2001*a*). Briefly, the microelectrode was filled with 2 M KCl with a tip resistance of 60–150 MΩ. Intracellular penetration was obtained by advancing the electrode into the adventitial surface of the vessel under

a stereo-microscope (Nikon SMZ-2T). Transmembrane potential and current were simultaneously monitored with an Axoclamp 2B preamplifier (Axon Instruments, Union City, CA, USA) or an npi SEC 10-LX preamplifier (npi electronic, Tamm, Germany). The electrical signals were recorded with a computer equipped with pCLAMP8 software (Axon Instruments) using sampling intervals of 0.1, 0.5 or 10 ms.

The resting potential was usually determined 5 min after the initial voltage jump at penetration and checked by the voltage jump at the withdrawal of the electrode. The input resistance was measured by applying 0.2–0.5 nA, 0.5–2 s current pulses via the recording electrode with the capacitance compensation and bridge balance well-adjusted on the npi preamplifier (Jiang *et al.* 2001*a*). Such adjustment was achieved by simultaneously using an additional data acquisition computer, a monitor displaying fast sweeps (0.5–2 s, Fig. 4) of *I–V* signals at a 10 kHz sampling rate. In addition, 5 or 10 sweeps were averaged to reduce the baseline noise. Transmural stimulus (0.4 ms, ± 10–20 V) was applied every 10 or 20 s via bipolar tungsten electrodes to evoke a junction potential (Jiang *et al.* 1999).

Histology and immunohistochemistry

The type of the cell recorded (SMC *versus* EC) and the dye-coupling were identified by intracellular dye injection and confocal microscopic examination (Emerson & Segal, 2000; Jiang *et al.* 2001*a*). Briefly, the sharp electrodes were tip filled with a fluorescent dye propidium iodide (1% in 2 M KCl), and back-filled with 2 M KCl. At the end of electrophysiological experiments, depolarizing pulses (0.5 nA, 20 ms, 16 Hz for 2 min) were applied to facilitate the dye diffusion. Then the SMA segment was mounted in a medium (Vectashield, Vector Laboratories Inc., Burlingame, CA, USA) with a coverslip for confocal fluorescence microscopic study (Bio-Rad MRC 1024 on a Nikon TE300) (Fig. 5).

Immunohistochemical staining for choline acetyltransferase (ChAT) was carried out on the SMA, and on the basilar artery (BA) and the anterior inferior cerebellar artery (AICA) for comparison (Fig. 7), and also on the organ of Corti to verify the sensitivity and specificity of the procedures (see Supplemental material Fig. 7-2). Briefly, tissues were isolated and fixed in 4% paraformaldehyde in 0.02 M phosphate-buffered saline (PBS; pH 7.4) for 2 h. After a wash with PBS, the specimens were immuno-blocked in 10% donkey serum and 1% bovine serum albumin in 0.02 M PBS (BSA-PBS) for 1 h. Tissues were incubated with goat-anti ChAT (affinity purified polyclonal antibody, Chemicon, 1 : 100 in BSA-PBS) for 48 h, and then incubated with Alexa-488-conjugated donkey antigoat I_gG (Molecular Probes, 1 : 100) for 3 h. The labelled tissues were mounted and observed on a Nikon Eclipse TE 300 microscope fitted with a Bio-Rad MRC 1024 confocal scanning laser microscopy system.

Drug application and statistics

Drugs of known concentrations were applied via the bathing solution. The solution that passed the recording chamber could be switched, without change in flow rate or temperature, to one that contained a drug or one of different ionic composition. Drugs used in this study were: acetylcholine (ACh), atropine, 4-diphenylacetoxy-*N*-methylpiperidine methiodide (DAMP), 1,2-bis(2-aminophenoxy)ethane-*N*,*N*,*N*′,*N*′-tetraacetic acid tetrakis acetoxymethyl ester (BAPTA-AM), glipizide, charybdotoxin (ChTX), apamin, ouabain, indomethacin, 17-octadecynoic acid (17-ODYA), and N^{ω}-nitro-L-arginine methyl ester (L-NAME), pyridoxal phosphate-6-azo(benzene-2,4-disulphonic acid (PPADS) (all from Sigma); 18β-glycyrrhetinic acid (18βGRA, ICN, USA) and propidium iodide (PI, Molecular Probe, Eugene, OR, USA). Statistical values are expressed as means ± S.E.M.

Results

Conventional intracellular recordings were made from more than 200 smooth muscle cells (SMCs) and endothelial cells (ECs) from more than 300 isolated SMA segments. The membrane properties of the cells are similar to those reported previously (Jiang *et al.* 2001*a*). Briefly, the cells sampled usually showed an initial resting potential either near −40 or −75 mV, called low and high RP, respectively. This is a bi-stable phenomenon since, during the recording period, a low RP cell may quickly shift its RP from the low level to the high level and vise versa (Fig. 1*A*; Jiang *et al.* 2001*a*).

Approximately equal numbers of SMCs and ECs were recorded in the present study. This is different from what we reported previously (Jiang *et al.* 2001*a*), in which more SMCs than ECs were recorded, probably because thin SMA segments (o.d. ∼50 μm) were more frequently used in the present study. The mean RP of the SMCs was slightly more negative than that of the ECs (−51 ± 2.6 mV, range from −30 to −88 mV, $n = 41$ and −41 ± 2.4 mV, range from −30 to −78 mV, $n = 43$, respectively). This was obviously because the ECs showed a higher ratio (39/4) of low RP/high RP cells than the SMCs (29/12, $P = 0.0264$, two-sided Fisher's exact test). The input resistance was also significantly different ($P < 0.01$, unpaired t test) between these two types of cells: 6.02 ± 0.78 MΩ, range 2.5–10.1 MΩ, for the ECs ($n = 11$) and 13.1 ± 1.8 MΩ, range 4.2–17.8 MΩ, for the SMCs ($n = 16$). Due to the large overlapping range, neither the RP level nor the input resistance could be used as a reliable index to determine the type of a cell.

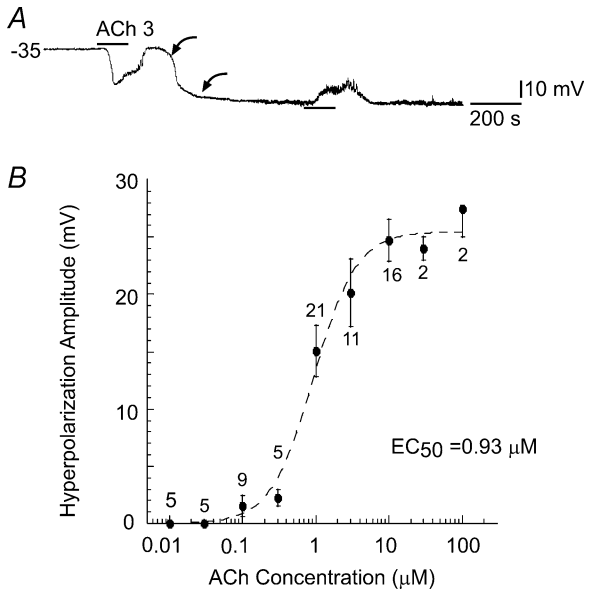

Figure 1. Acetylcholine causes a hyperpolarization in cells with a low resting potential
A, ACh (3 μM) induced a hyperpolarization in a cell that initially had a low resting potential (less negative than −60 mV; Jiang *et al.* 2001*a*), but caused a depolarization after the cell shifted (between two curved arrows) to a high resting potential. *B*, the amplitude–concentration plot of ACh-hyperpolarization fitted with Michaelis-Menten equation reveals an EC_{50} of 0.93 μM.

Membrane actions of acetylcholine

Bath application of ACh (0.1–10 μM) caused a hyperpolarization in almost all the cells that had a low RP (−30 to −60 mV, $n = 134$, Fig. 1*A*). The hyperpolarization often had a fast transient phase lasting about 1–3 s, followed by a sustained phase which lasted to the end of the application (Figs 1*A* and 2). These two phases were sometimes separated by a narrow notch (Figs 2*A* and 6*D*), or they merged as a single phase (Figs 1*A* and 2*B* and *C*). The washout recovery of the membrane potential often had a fast and a slow phase, completing within 2–4 min. The maximum amplitude of the ACh-induced hyperpolarization, measured at slow phase, was concentration dependent (Fig. 1*B*), with an EC_{50} of 0.93 μM and a Hill coefficient of 1.49. Repeated application of high concentrations (10 μM) at an interval of less than 15 min often caused a run-down of the response. ACh (1–10 μM)-induced hyperpolarization was completely blocked by atropine (100 nM, $n = 5$, not shown) or an M_3 receptor-selective antagonist, DAMP (50 nM, Fig. 2*A* and *E*). The blockade was reversible upon washout of the antagonist (60 and 20 min for atropine and DAMP, respectively).

In more than 10 cells, the hyperpolarization induced by 1–10 μM ACh did not recover; instead, the

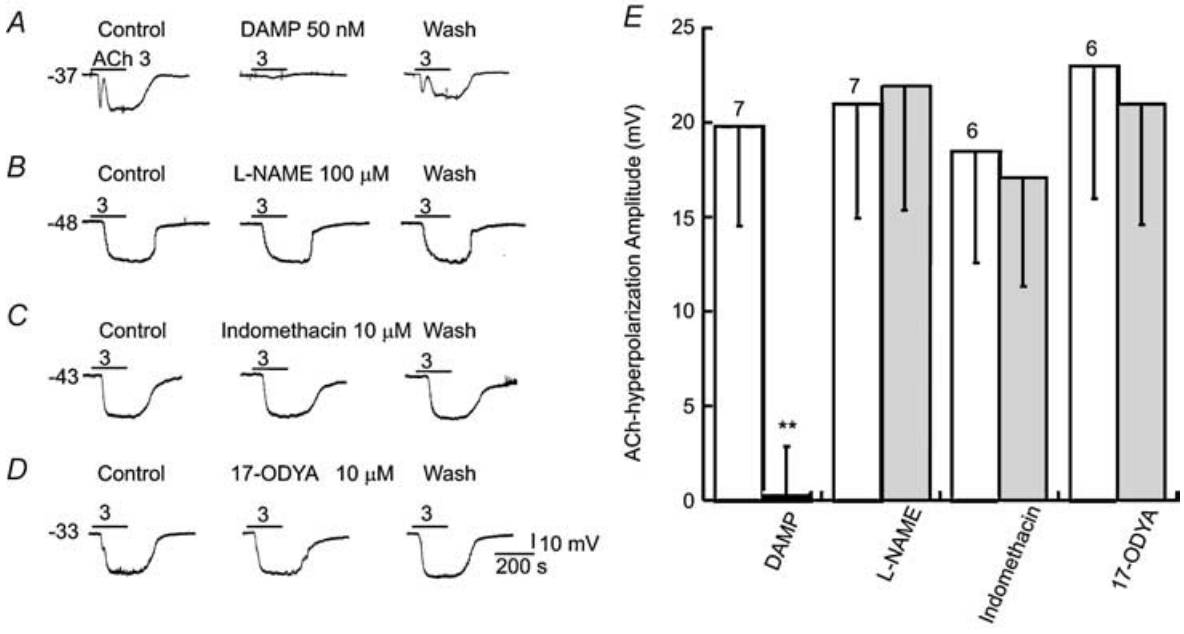

Figure 2. Hyperpolarization by ACh was blocked by M_3 muscarinic receptor antagonist but not by NOS, cyclo-oxygenase or cytochrome P450 inhibitors
A, the 3 μM ACh-hyperpolarization was reversibly blocked by 50 nM DAMP in an identified EC. *B–D*, NOS inhibitor L-NAME, cyclo-oxygenase inhibitor indomethacin and cytochrome P450 inhibitor 17-octadecynoic acid (17-ODYA) had no significant effects on the ACh-hyperpolarization. DAMP, indomethacin and 17-ODYA themselves caused no membrane potential changes whereas L-NAME induced small depolarization in some cells (not shown). *E*, column plot of data statistics, showing a significant (**$P < 0.01$, paired *t* test) inhibition only by 50 nM DAMP. The open columns are controls. The number of cells tested are indicated above each column pair.

hyperpolarization remained and further shifted to a hyperpolarized level near −75 mV for the rest of recording time, for up to 3 h (also see (Jiang *et al.* 2001*a*). When the cell originally had or shifted to such a high RP, ACh always induced a depolarization (Fig. 1*A*). The depolarization was apparently not simply a reversed hyperpolarization due to the RP change; rather the ACh-induced hyperpolarization and depolarization were two events generated by different channel activities since the hyperpolarization but not the depolarization was blocked by ChTX (Fig. 3*A*, also see (Jiang *et al.* 2004). We will address the ACh-induced depolarization in detail in another report.

ACh-hyperpolarization is independent of releasing NO or products of cyclo-oxygenase and cytochrome P450

Application of L-NAME (100–300 μM), an isoform-non-specific nitric oxide synthase (NOS) inhibitor, failed to inhibit the ACh-induced hyperpolarization in all seven cells tested (Fig. 2*B* and *E*). Neither did the K_{ATP} channel blocker glipizide (3–5 μM) inhibit the ACh-induced hyperpolarization ($n = 4$, not shown).

The cyclo-oxygenase inhibitor indomethacin (10–50 μM) or the selective EET-production inhibitor 17-octadecynoic acid (10 μM) had no significant effect on ACh-induced hyperpolarization in all cells tested (Fig. 2*C*, *D* and *E*, $n = 6$). Other cytochrome P450 inhibitors such as clotrimazole and (+)-miconazole nitrate were not used because they directly inhibit Ca^{2+}-dependent and Ca^{2+}-independent voltage-gated K^+ currents in arterial myocytes (Yuan *et al.* 1995).

K^+ channel mediation of ACh-hyperpolarization

ACh-hyperpolarization was substantially (60–90%) blocked by the K_{Ca} blocker charybdotoxin (ChTX, 50 nM; 81 ± 5.4%, $n = 5$, $P < 0.05$, paired t test), and addition of 100 nM apamin caused additional 10–20% blockade ($n = 3$, Fig. 3*A*). The blockade was reversible after 20–40 min wash with toxin-free solution. The voltage-dependent K^+ channel (K_V) blocker 4-AP (0.1 and 1 mM) had no significant effect on the ACh-hyperpolarization ($n = 6$). In addition, the ACh-hyperpolarization (1–3 μM) was quickly abolished (80–100% in 5–7 min) by bath application of a membrane-permeant Ca^{2+} chelator, BAPTA-AM (50 μM, $n = 6$, Fig. 3*B*). The response largely recovered after 10–20 min washout if the application time of BAPTA-AM was less than 7 min.

ACh (10 μM)-induced hyperpolarization was smaller (18.8 ± 2.0 mV, $n = 9$) in cells that had a RP between −60 and −45 mV than that (30.2 ± 0.7 mV, $n = 39$) in cells that had a RP from −44 to −25 mV ($P < 0.05$, t test). A linear fit to the plots of ACh-hyperpolarization amplitude against the RP of all the cells revealed a slope of 0.3.

The input resistance (R_{input}) was decreased to 7.8 ± 1.2 MΩ in the sustained phase of 3 μM ACh-hyperpolarization from a control of 9.1 ± 1.2 MΩ ($P < 0.05$, $n = 10$, paired t test, Fig. 4). The barium ion (Ba^{2+}, 50–100 μM), a K_{ir} blocker, did not significantly inhibit ACh-hyperpolarization in identified ECs but had about 30% inhibition on the ACh response in the identified SMCs (see next section, Fig. 6). In the presence of 50 μM Ba^{2+}, the R_{input} during the 10 μM ACh-induced hyperpolarization was also significantly reduced to 10.4 ± 3.6 MΩ from the control of 13.2 ± 3.8 MΩ ($n = 6$, $P < 0.05$, paired t test). Figure 4 also shows that the R_{input} decrease during the ACh-hyperpolarization was not significantly affected by 18β-glycyrrhetinic acid (18βGRA) in the identified EC ($n = 3$). The gap junction blocker alone significantly increased input resistance by 159% (to 28.7 ± 5.35 MΩ from a control of 11.1 ± 1.21 MΩ, $n = 7$, $P < 0.05$, paired t test, Fig. 4).

Origin of ACh-induced hyperpolarization: the SMC *versus* the EC

After excluding possible mediations by NO and products of cyclo-oxygenase and cytochrome P450, it is reasonable

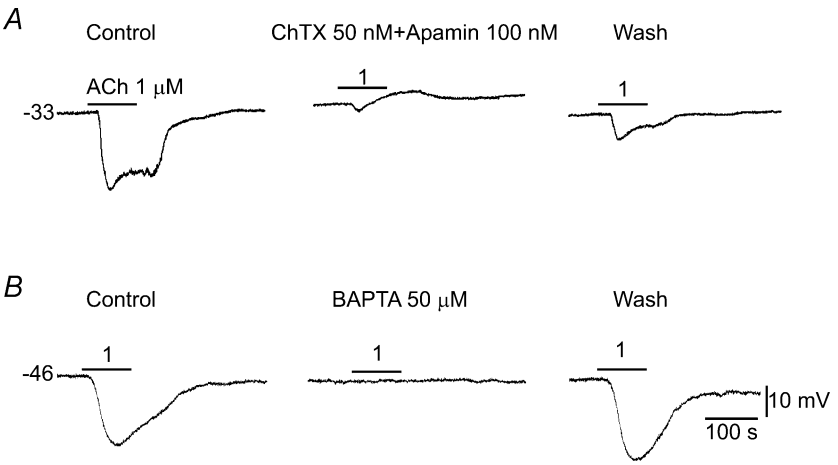

Figure 3. Mediation by Ca^{2+}-activated potassium channels of the ACh-hyperpolarization
Sample recordings show that a combination of charybdotoxin (ChTX) and apamin (*A*), or BAPTA-AM (*B*) near-completely abolished the ACh-induced hyperpolarization. Note that, in *A*, an ACh-induced depolarization was unmasked by the presence of ChTX and apamin while the initial fast phase of hyperpolarization was partially suppressed. The toxins and BAPTA-AM often caused a small (3–6 mV) depolarization. *A* and *B* are from different preparations. The cell of *A* was identified as an EC (see Fig. 5).

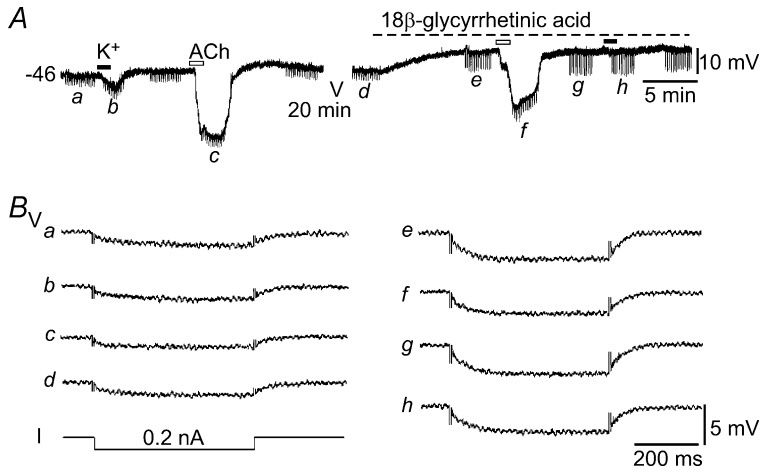

Figure 4. ACh-hyperpolarization associated with a decrease in input resistance
A, a trace showing the membrane potential responses of an EC to 10 mM K^+ and 3 μM ACh, with and without the presence of 25 μM 18β-glycyrrhetinic acid (18βGRA). The input resistance was measured by transmembrane current pulses (I, 0.2 nA, 500 ms) in 20 s intervals when needed (*a–h*). *B*, fast sampled (10 kHz) traces *a–h* were averages of all 10 sweeps of potential responses to the current pulses applied as labelled in *A*. Note that the input resistance was reduced to 9 and 7.8 MΩ by high K^+ and ACh, respectively, from the control of 10.5 MΩ in this cell. In the presence of 25 μM 18βGRA, which increased the input resistance to 20.6 MΩ, ACh decreased the input resistance to 16.9 MΩ, whereas high K^+ caused little change in the input resistance during the high K^+ application where the K^+-induced hyperpolarization was near-completely suppressed by 18βGRA.

to hypothesize that the ACh-induced hyperpolarization in the SMC is co-mediated from the ECs by two pathways: one via electrical coupling and the other via EC release of K^+ that in turn causes K_{ir} activation and hyperpolarization in the SMC. To further test this hypothesis and to address the possible non-specific effect of 18βGRA (Coleman *et al.* 2001*b*), three groups of experiments were conducted.

First, we re-examined the possible myoendothelial dye coupling, using confocal microscopy rather than the conventional fluorescence microcopy as used before (Jiang *et al.* 2001*a*). Similarly to a previous report (Jiang *et al.* 2001*a*), the recorded cell often showed a strong staining of the rod-shaped nucleus after recording with the propidium iodide-containing electrode (Fig. 5). The cell type (SMC *versus* EC) could be identified by the orientation of the rod-like nucleus to the vessel. From preparations that had a long-lasting (> 30 min) single cell recording, we frequently found that, in addition to the strongly stained EC or SMC, there were 1–12 faintly stained cells of both types adjacent to the strongly stained cell (Fig. 5), suggesting that the dye injected into the recorded cell was variably transferred to the adjacent cells.

Second, we estimated the myoendothelial electrical coupling efficiency in the SMA by taking advantage of the lack of K_{ir} expression in the EC in most arterioles (Nilius & Droogmans, 2001), which is also the case in the SMA as we suggested previously (Jiang *et al.* 2001*a*). We first tested again the effects of 25 μM 18βGRA on

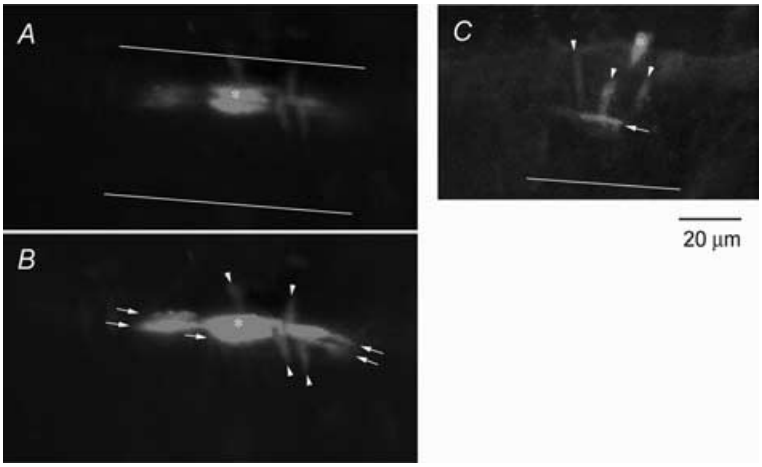

Figure 5. Dye coupling in the SMA revealed by confocal microscopy
Single cells (*) were recorded for 170 min (*A* and *B*) and 75 min (*C*) with a microelectrode containing 1% propidium iodide. *A*, single optic slice crossing the most densely stained cell shows a nucleus having an orientation parallel to the vessel axis, indicating that the recorded cell is an endothelial cell. The continuous lines indicate the edges of the vessel (also in *C*). *B*, reconstructed image of 10 consecutive optic slices of 3 μm intervals from the same specimen of *A* showing that at least 4 smooth muscle cells (arrowheads) and 5 endothelial cells (arrows) received various amount of transferred dye molecules from the recorded endothelial cell. *C*, reconstructed image of another preparation showing that at least 3 SMCs and 1 EC were dye-coupled to a recorded smooth muscle cell; the latter was identified by its circumferential orientation to the vessel axis.

Table 1. Inhibition of K^+- and ACh-induced hyperpolarization by Ba^{2+} and ouabain in endothelial cells *versus* smooth muscle cells

	Endothelial Cells				Smooth muscle cells			
	Control	In Ba^{2+} (100 μM)	Control	In Ba^{2+} + ouabain (1 μM)	Control	In Ba^{2+} (100 μM)	Control	In Ba^{2+} + Ouabain (1 μM)
High K^+-induced hyperpolarization (mV)	10.2 ± 3.1	1.52 ± 0.8*	11.4 ± 2.5	0.68 ± 0.72**	24 ± 2.2*	4.2 ± 2.4**	25 ± 2.7	1.8 ± 0.81**
(Δ%)	—	(−85.1%)	—	(−94%)	—	(−82.5%)	—	(−93%)
n	16	16	8	8	16	6	5	5
ACh-induced hyperpolarization (mV)	28.6 ± 2.0	28.2 ± 2.7	27.2 ± 2.6	23.2 ± 2.4	29 ± 2.8	20 ± 0.8**	23 ± 3.8	9.3 ± 1.7**
(Δ%)	—	(−1.4%)	—	(−15%)	—	(−31%)	—	(−60%)
n	12	12	6	6	8	8	5	5

*$P < 0.05$, **$P < 0.01$, paired *t* test between the treatment column and its control, unpaired *t* test between the initial controls of the EC and the SMC.

Table 2. Inhibition of K^+- and ACh-induced hyperpolarization by ouabain and Ba^{2+} in endothelial cells *versus* smooth muscle cells

	Endothelial Cells				Smooth muscle cells			
	Control	In ouabain (1 μM)	Control	In ouabain + Ba^{2+} (100 μM)	Control	In ouabain (1 μM)	Control	In ouabain + Ba^{2+} (100 μM)
High K^+-induced hyperpolarization (mV)	13 ± 1.6	8.5 ± 2.9*	12 ± 1.9	0.33 ± 0.62**	22 ± 1.5*	18 ± 2.0*	23 ± 2.1	1.0 ± 0.60**
(Δ%)	—	(−35%)	—	(−97%)	—	(−19%)	—	(−96%)
n	12	12	9	9	13	13	9	9
ACh-induced hyperpolarization	23 ± 2.4	21 ± 3.1	23 ± 3.7	13 ± 3.4**	20 ± 2.9	14 ± 3.9*	20 ± 3.3	6.1 ± 2.1**
(Δ%)	—	(−8.7%)	—	(−42%)	—	(−31%)	—	(−69%)
n	13	13	6	6	12	12	9	9

*$P < 0.05$, **$P < 0.01$, paired *t* test between the treatment column and its control, unpaired *t* test between the initial controls of the EC and the SMC.

10 mM K^+-induced hyperpolarization in dye-identified cells as we reported previously (Jiang *et al.* 2001*a*). We found that the gap junction blocker 25 μM 18βGRA near-completely blocked the high K^+-hyperpolarization in all the ECs tested ($n = 6$, Fig. 4) but had no significant effect on high K^+-hyperpolarization in the SMCs ($n = 5$, also see Supplementary material Table 1 for summary of accumulative data), consistent with the notion that the high K^+-induced hyperpolarization originates from the SMCs, that the EC expresses no K_{ir} channels and that its high K^+-induced hyperpolarization was an electrical spread from the SMCs. Then we found that the 10 mM K^+-induced hyperpolarization in the ECs (11.4 ± 2.3 mV, $n = 28$) was significantly smaller ($P < 0.05$, *t* test) than that in the SMCs (23.1 ± 1.48 mV, $n = 29$, Tables 1 and 2), indicating a macroscopic SMC-to-EC coupling efficiency of 0.49 (11.4/23.1). It was also notable that the amplitude of high K^+-hyperpolarization was much more variable in ECs than in SMCs, consistent with the notion that a heterogeneous coupling exists between the ECs and SMCs (Jiang *et al.* 2001*a*).

Third, we compared the amplitudes of ACh-hyperpolarization between the SMC and the EC. The amplitudes of 3 μM ACh-induced hyperpolarization were 23.6 ± 2.24 mV and 25.6 ± 1.52 mV in the SMCs ($n = 20$, RP $= -41.1 \pm 0.57$ mV) and ECs ($n = 25$, RP $= -39.4 \pm 0.76$ mV), respectively, with no significant difference between the two cell types ($P > 0.05$, Tables 1 and 2), indicative of a mechanism(s) additional to the electrocoupling may involve in the ACh-hyperpolarization in the SMC (see Discussion). The waveform of the ACh-hyperpolarization was not significantly different between these two cell types either.

Role of K_{ir} and Na^+–K^+ pump current activation

Five groups of experiments were conducted to estimate the role of K_{ir} and pump current activation in ACh-hyperpolarization in the SMC.

(1) Ba^{2+} (100 μM) suppressed 10 mM K^+-induced hyperpolarization in all the SMCs and ECs tested by 82.5% and 85.1%, respectively (Fig. 6*A*–*D*, Table 1);

addition of ouabain (1–10 μM) near-completely abolished the high K^+-hyperpolarization (Fig. 6*A* and *C*, Table 1). Ba^{2+} alone induced a depolarization in all the SMCs (7.1 ± 0.66 mV, $n = 8$) and the ECs tested (5.8 ± 0.22 mV, $n = 16$). Ouabain alone or in the presence of Ba^{2+} also caused a depolarization in both ECs and SMCs (Fig. 6*A* and *C* and 8.2 ± 1.6 mV and 10.5 ± 2.6 mV, $n = 24$ and 23, respectively).

(2) Application of 1 μM ouabain alone inhibited the high-K^+-hyperpolarization by 19.4% in the SMC and 34.6% in the EC (Table 2). Addition of Ba^{2+} also caused near complete inhibition of the high-K^+-hyperpolarization in both cell types (Table 2). The significantly stronger inhibition by ouabain on high-K^+-hyperpolarization in ECs than in SMCs is suggestive of a gap junction blockade (Martin *et al.* 2003), and this was further supported by input resistance measurements. Ouabain (1 μM) caused a ~50% increase in input resistance (from a control of 8.3 ± 2.1 MΩ to 12.2 ± 2.3 MΩ, $P < 0.05$, paired t test) in seven cells tested. Taken together, our data (Fig. 6, Tables 1 and 2) suggest that activation of K_{ir} and pump current plays a role at roughly an 8 : 1 ratio in the high-K^+-induced hyperpolarization in the SMC (see Discussion).

(3) The ACh-induced hyperpolarization in SMCs was significantly attenuated (−31%) by 100 μM Ba^{2+} (Fig. 6*A* and *B*, Table 1). In contrast, 100 μM Ba^{2+} did not significantly change the 3 μM ACh-induced hyperpolarization in ECs (Fig. 6*C* and *D*, Table 1). In 100 μM Ba^{2+}, ouabain (1–10 μM) caused significant additional (29.4%) inhibition (total 60.3%) of the ACh-hyperpolarization in the SMCs (Fig. 6*A*, Table 1), whereas the addition of ouabain only slightly (15%) inhibited the amplitude of ACh-hyperpolarization in the ECs (Fig. 6*C*, Table 1).

(4) Ouabain (1 μM) alone reduced ACh-hyperpolarization by 31% ($P < 0.05$) in the SMC but by 8.7% ($P > 0.05$) in the EC (Table 2), which is again consistent with a gap junction blockade. Addition of Ba^{2+} caused a significant additional inhibition of ACh-hyperpolarization in the ECs (by 33%) and SMCs (by 38%), or a total inhibition of ACh-hyperpolarization by 42% in the EC and by 69% in the SMC (Table 2).

(5) A combination of 100 μM Ba^{2+} with 18βGRA (25 μM) near completely blocked the ACh-hyperpolarization in the identified SMCs (Fig. 6*B*, $n = 5$), but not in the ECs (Fig. 6*D*, $n = 5$). In some SMCs (Fig. 6*B*, $n = 2$), an ACh-depolarization was unmasked after suppression of the hyperpolarization.

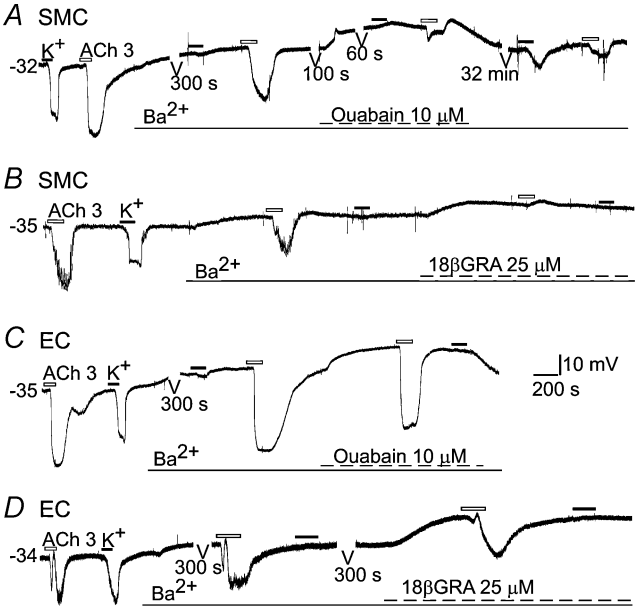

Figure 6. ACh-hyperpolarization in smooth muscle cells was partially blocked by Ba^{2+} and completely blocked by additional 18βGRA

Cells are from tracer-identified SMC or EC. Note that Ba^{2+} (100 μM) strongly blocked 10 mM K^+-induced hyperpolarization in both types of cells (*A–D* and *F*), but only partially suppressed the ACh-hyperpolarization in SMCs (*A, B* and *E*) and had no significant inhibition on the ACh-hyperpolarization in ECs (*C* and *D*). Addition of ouabain further reduced the ACh-hyperpolarization in the SMC (*A*) but had little effect on the amplitude of ACh-hyperpolarization in the EC (*C*). ACh-hyperpolarization was almost completely blocked by a combination of Ba^{2+} and a gap junction blocker 18βGRA in the SMC (*B*) but not in the EC (*D*). Gaps in traces (*A*, *C* and *D*, 60 s to 32 min) were omitted segments of continuous recording for clarity.

Immunohistochemical staining of ChAT fibres and evoked junction potential

We hypothesized that the SMA may receive cholinergic innervation based on such robust membrane effects of ACh described above and a report that muscarinic antagonists reduce cochlear blood flow (Suga & Snow, 1969). Cholinergic fibres were examined by polyclonal antibody to acetyltransferase (ChAT) on the SMA as well as on its upstream arteries, basilar artery (BA) and anterior inferior cerebellar artery (AICA) in three guinea-pigs (Fig. 7). In all the specimens examined, ChAT-immunoreactive fibres form a sparse plexus along the vessel with varicosities *en route* or at the end of fibres. All the fibres are very fine (< 0.5 μm). The density of fibres was estimated to be about one-fifth that of tyrosine hydroxylase positive fibres (Jiang *et al.* 1999). When a blocking peptide was present or the anti-ChAT antibody was replaced by bovine serum albumin, no fluorescent fibres were seen, suggesting a good specificity of the staining procedures. The specificity and sensitivity of the antibody and the staining procedure used were also confirmed on guinea-pig cochlea where the known cholinergic efferent fibres and terminals were strongly stained with ChAT antibody (see Supplemental material Fig. 7-2).

Transmural single stimulus (8–20 V, 0.4 ms) induced a TTX-sensitive excitatory (depolarizing) junction potential (EJP) in the majority of cells recorded as we previously described (Fig. 7*J*; Jiang *et al.* 1999). Of 98 cells (51 and 47 being low and high RP cells, respectively, and 10 and 13 being identified as the EC and SMC, respectively), all showed an evoked excitatory junction potential (2–28 mV) while none of them showed an inhibitory or biphasic junction potential. An inhibitory (hyperpolarizing) junction potential remained undetected when an EJP in low RP cells was largely blocked by combined antagonists prazosin (0.1 μM), idazoxan (0.1 μM) and PPADS (10 μM) for α_1, α_2 and P_{2X} receptors, respectively ($n = 15$). On the other hand, a muscarinic receptor antagonist, 4-DAMP (50 nM), reversibly attenuated the evoked EJP by $37.4 \pm 4.31\%$ (range 21–62%, $n = 10$, Fig. 7*J*) in about half of the cells tested ($n = 23$). The EJPs of the remaining 13 cells were not changed by 4-DAMP.

Discussion

The main finding of the present study is the quantitative demonstration of a co-mediation mechanism of the ACh-induced hyperpolarization in the vascular smooth muscle cells, i.e. in addition to electrical coupling via myoendothelial gap junctions that allow ACh-induced hyperpolarization in the ECs to spread to SMCs (Jiang *et al.* 2001*a*), a K^+ release from the endothelium, and thus activation of K_{ir} and pump current in the SMCs. We estimated these two pathways share roughly 60% and 40% contributions, respectively (see next). To the best of our knowledge, this is the first analysis that quantified the combined mechanism of myoendothelial electrical coupling and endothelial K^+ release in arterioles. The other tested diffusible molecules, including NO, cyclo-oxygenase and cytochrome P450 products, are not involved in the ACh-hyperpolarization in the vessel investigated.

K_{Ca} mediation of the ACh-hyperpolarization

Our data support the notion that the ACh-induced hyperpolarization in SMA ECs is generated by opening of K_{Ca} that is somehow coupled to ACh receptor. Evidence includes: (1) the hyperpolarization was associated with an increase in input conductance (decrease in input resistance); (2) the amplitude of hyperpolarization was increased in cells with less negative RP and decreased in cells with more negative RP; and (3) the hyperpolarization was blocked by the K_{Ca} channel blockers ChTX and apamin, and by membrane-permeant Ca^{2+} chelator but not by blockers selective for other K^+ channels including Ba^{2+} for K_{ir} (in ECs), glipizide for K_{ATP}, and 4-AP for K_V (Hille, 2001; Nilius & Droogmans, 2001).

Large, small and intermediate conductance K_{Ca} have all been identified in the endothelial cell (Nilius & Droogmans, 2001). Agonists such as ACh and bradykinin may activate an intermediate conductance K_{Ca} (IK_{Ca}) that has a single channel conductance between 30 and 80 pS and is sensitive to ChTX (Van Renterghem *et al.* 1995). More experiments are needed to determine the subtype(s) of K^+ channels that mediate the ACh-hyperpolarization in the SMA.

Myoendothelial dye coupling

In the literature, dye coupling between vascular SMCs and ECs has only been seen in a few studies using small molecular mass dyes (Little *et al.* 1995; Beny *et al.* 1997), although tracer coupling has been demonstrated to be strong within endothelial layers and weaker between the SMCs in many arteries including the SMA (Emerson & Segal, 2000; Coleman *et al.* 2001*b*; Jiang *et al.* 2001*a*;

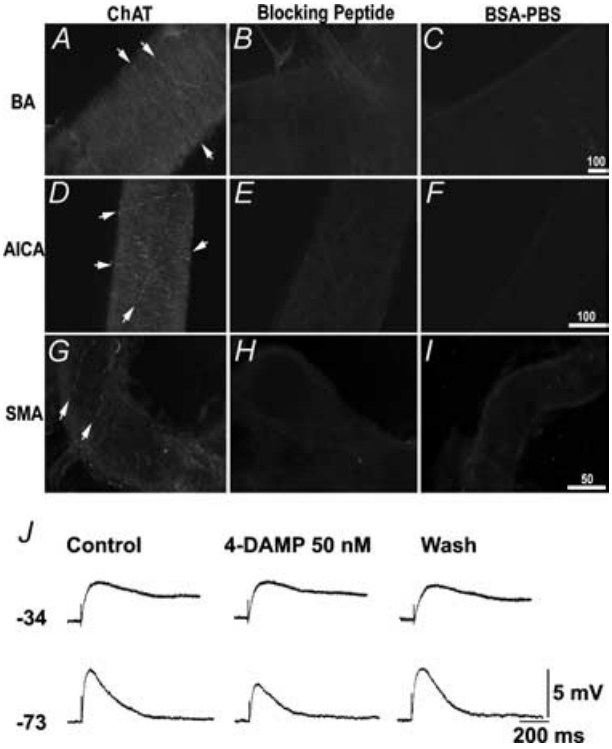

Figure 7. ChAT expression in the arteries and 4-DAMP-sensitity of the excitatory junction potential (EJP) in the SMA
A–I, micrographs showing that ChAT-immunoreactive fibres (bright red) were present in basilar artery (BA) (*A*), anterior-inferior-cerebellar artery (AICA) (*D*) and SMA (*G*). Note that ChAT-labelled nerve fibres and varicosities form a sparse plexus (arrows). When the vessels were incubated with a medium containing blocking peptide-adsorbed ChAT antibodies, negligible labelling was noted in all the vessels tested (*B, E* and *H*). When primary antibody was replaced by BSA-PBS, no labelling was observed (*C, F* and *I*). Scale bars in micrometres. *J*, traces showing EJPs recorded from two cells having low and high RP, respectively, in the SMA. The M_3 receptor-selective antagonist 4-DAMP, significantly attenuated the EJP in the cell that had a high RP cell (bottom traces) but not in the other (upper traces). Each trace was an average of 5 sweeps. The stimulus artifact was truncated for clarity.

Yamamoto *et al.* 2001). The frequent failure, including ours (Jiang *et al.* 2001*a*), to find the myoendothelial dye coupling has been attributed to the gap junction properties, and the molecular size and electrical charge of the tracer used (Little *et al.* 1995; Beyer *et al.* 2000). For instance, Lucifer yellow was confirmed to be poorly permeant through smooth muscle gap junctions (Emerson & Segal, 2000), whereas all tested dyes were well transferred between endothelial cells. The present demonstration of myoendothelial dye coupling (Fig. 5) has added an another parameter to the interpretation of the negative findings, i.e. the optic and/or photic resolution of the regular fluorescence microscopy seems inadequate for examination of the faintly stained coupled cells, at least when the fluorescent dye PI is used (Emerson & Segal, 2000; Jiang *et al.* 2001*a*).

Role of electrical coupling *versus* endothelial K^+ release in muscular ACh-hyperpolarization

The present demonstration of myoendothelial dye coupling supports the notion that the ACh-hyperpolarization originates from the endothelium and then electrotonically spreads to muscle cells via gap junctions. Moreover, our data show that the amplitude of ACh-hyperpolarization in the SMA was nearly as big as that in the EC but the gap junction coupling was relatively weak, suggesting an additional mechanism(s) may be involved in generating the ACh-hyperpolarization in the SMCs. Ba^{2+} ($\leq$100 μM) is a selective K_{ir} blocker (Quayle *et al.* 1997; Jiang *et al.* 2001*a*) and has no effect on gap junction conductance (Spray & Bennett, 1985; Ceelen *et al.* 2001). Barium (100 μM) largely blocked 10 mM K^+-induced K_{ir} activation and hyperpolarization in both SMCs and ECs (Fig. 6, Table 1) while a combination of 100 μM Ba^{2+} with 18βGRA near-completely blocked the hyperpolarization in SMCs. A logical interpretation of these results would be that, in 18βGRA, the remaining 16% of ACh-hyperpolarization in the SMCs is due to a K^+ elevation in myoendothelial space.

Our other experiments indicate that the K^+ elevation probably contributes more than 16% of the ACh-hyperpolarization in the SMC. First, we observed that 100 μM Ba^{2+} inhibited 31% of the ACh-hyperpolarization in the SMC but had little effect in the EC (Table 1). Secondly, the 31% inhibition is likely to be an underestimate since Ba^{2+}-induced depolarization should have increased the driving force for K_{Ca}-mediated hyperpolarization, and the latter would have offset the Ba^{2+}-induced inhibition. Based on Ba^{2+} induced $\sim$7 mV depolarization in the SMC and the response/RP slope of 0.3, such offset may amount to 2.1 mV. If we include this estimate in the results, Ba^{2+} would have inhibited 35.7% [(20 – 29 – 2.1)/(29 + 2.1) mV] of the ACh-hyperpolarization in the SMC. Thirdly, considering that 100 μM Ba^{2+} inhibits only $\sim$85% of the K^+-induced hyperpolarization, the total K^+-release-related hyperpolarization would be 42% (35.7%/0.85). This calculation is pertinent because data (Table 1) show that Ba^{2+} has almost equal inhibition ($\sim$85%) of K^+-hyperpolarization in both cell types. Also, the ACh-induced K^+ elevation in the myoendothelial interstitial space might be approximately mimicked by 10 mM K^+ application. In the SMA, an extracellular K^+ elevation to 20 mM or higher often causes depolarization after a brief hyperpolarization in the low RP cells (see Fig. 4 of Jiang *et al.* 2001*a*). In this respect, the myoendothelial space K^+ was raised to $\sim$10 mM by 10 μM ACh from a control level of 4.6 mM in rat hepatic arterioles (Edwards *et al.* 1998).

Taken together, we believe that roughly 40% of ACh-hyperpolarization in the SMC is due to K^+ release and the remaining 60% should be attributed to electric coupling. The 84% inhibition by 18βGRA may thus reflect a significant non-specific inhibition (Coleman *et al.* 2001*a*) in addition to its gap junction blocking effect. A significant depolarization by 18βGRA in both the EC and the SMC in the SMA also signified a non-specific action. Our myoendothelial coupling efficiency measurement (0.49) also indicates that the 85% interlayer transmission efficiency is unlikely. The coupling efficiency of 0.49 in the SMC-to-EC direction is about a half of that (0.92) in guinea-pig mesenteric arterioles (Yamamoto *et al.* 2001), suggesting that the SMA may also have a weaker coupling in the EC-to-SMC direction than mesenteric arterioles (0.8).

Role of K_{ir} *versus* pump current activation in muscular ACh-hyperpolarization

Elevation of extracellular K^+ also activates the electrogenic Na^+–K^+ pump that causes hyperpolarization (Edwards *et al.* 1998, 1999*b*). The additional ouabain blockade (30.4%) on the ACh-hyperpolarization in the SMC in the presence of Ba^{2+} is consistent with this notion. However, a total of 60% inhibition by Ba^{2+} plus ouabain apparently presented an overlap with the electric coupling efficiency of 0.49. We believe this 60% is probably an overestimate of K^+-induced component in the ACh-hyperpolarization in the SMC due to a side-effect(s) of ouabain additional to its pump current suppression (see below).

Our data in two ways support the notion that ouabain may exert an inhibitory action on gap junction conductance as suggested by others (Martin *et al.* 2003). First, in contrast to Ba^{2+} equally inhibiting high K^+-hyperpolarization in both types of cells, ouabain blocked K^+-hyperpolarization by 19% in the SMC and by 35% in the EC (Table 2). Second, ouabain consistently increased the input resistance of the cells recorded. If the same amount of gap junction blockade by ouabain would happen in the EC-to-SMC direction, we could expect that the ouabain inhibition of ACh-hyperpolarization in

the SMC would be 16% larger than that in the EC, i.e. 9% + 16% = 25% (Table 2). This is comparable with the actual measurement (31%). In addition, ouabain is expected to time-dependently increase intracellular Na^+ and decrease intracellular K^+, which will positively shift the equilibrium potential for K^+ and reduces the ACh-hyperpolarization. On the other hand, the Ba^{2+} concentration (100 μM) we chose in the analysis showed a maximal K_{ir} inhibition (Fig. 6) but retained a good specificity, e.g. it has little effect on K_{Ca} and K_{ATP} in the SMA (Fig. 6; Jiang *et al.* 2001*a*; Si *et al.* 2002) and in other arterioles (Coleman *et al.* 2001*b*). Based on these findings, Ba^{2+} appears a much better agent than ouabain as the tool to analyse the role of K^+ elevation in membrane responses.

When applied in different sequence, Ba^{2+} and ouabain showed different potency on K^+-hyperpolarization. With Ba^{2+} applied first, 85% and 96% K^+-hyperpolarization was inhibited by Ba^{2+} and by Ba^{2+} plus ouabain, respectively, in both the EC and SMC suggesting an 8 : 1 role ratio of K_{ir}/pump current in the K^+-hyperpolarization. On the other hand, with ouabain applied first, ouabain and ouabain plus Ba^{2+} inhibited K^+-hyperpolarization by 19% and 96%, respectively, in the SMC, suggesting a roughly 4 : 1 role of K_{ir}/pump current in the K^+-hyperpolarization. The mechanism for such an overlapping action between these two compounds is not fully known at this moment. The ouabain-induced depolarization and initial inhibition of hyperpolarization, however, are expected to exert some inhibition on the K_{ir}-mediated hyperpolarization. The role of K_{ir} *versus* pump current should anyhow be between 8 : 1 and 4 : 1, maybe closer to 8 : 1 since Ba^{2+} has a better specificity than ouabain.

Physiological significance

Identification of the ChAT-immunoreactive fibres in the SMA supports the notion that ACh may function as a neurotransmitter in this vessel, as in guinea-pig choroid arterioles (Hashitani *et al.* 1998). Our failure to find an inhibitory junction potential to single or a short train of electrical stimuli (Jiang *et al.* 1999) may not be evidence against the possible cholinergic transmission. It is known that vascular nerve fibres are confined to the outer or adventitial layer (tunica adventitia) and some make specialized contact with the muscle cells in the media layer (Hirst *et al.* 1996). It is understandable that the ACh released from nerve terminals may not reach a sufficient amount to diffuse to and stimulate the muscarinic receptor on the EC in the inner layer of the vessel. On the other hand, that the M_3 receptor antagonist 4-DAMP significantly (~40%) inhibited the evoked EJP in about half of the cells supports the possible cholinergic transmission. Lack of inhibition by 4-DAMP in half of the cells could be due to a combination of factors such as (1) lack of cholinergic innervation in these cells (all the ECs and maybe some SMCs), as the ChAT-immunoreactive fibres are sparse; (2) the cells being poorly coupled to those that receive cholinergic innervation, and (3) the low RP cells usually having a smaller ACh-induced depolarization than the cells that showed a high RP (Jiang *et al.* 2004). Taken together, our data support a tentative cholinergic transmission in the SMA but the cellular mechanism underlying the cholinergic control of cochlear blood flow detected *in vivo* (Suga & Snow, 1969) remains to be clarified.

In summary, we presented electrophysiological and histological data suggesting that, in guinea-pig spiral modiolar artery, ACh directly stimulates muscarinic receptor and hyperpolarizes the endothelial cells by activating K_{Ca} channels. ACh indirectly hyperpolarizes the muscle cells by two pathways: (1) electrotonic spread of the endothelial hyperpolarization to the muscle cells via gap junctions and (2) the endothelial K^+ release that activates the K_{ir} and Na^+–K^+ pump current in SMCs, functioning at about 60% *versus* 40% ratio in the *in vitro* SMA. K_{ir} and Na^+–K^+ pump current activation may be responsible for K^+-release-induced hyperpolarization at up to 8 : 1 ratio. Since heterogeneity in the nature of the EDHF has been repeatedly reported among vascular preparations, the EDHF mechanisms reported here may not be applicable to other systemic arteries.

References

Beny JL, Zhu P & Haefliger IO (1997). Lack of bradykinin-induced smooth muscle cell hyperpolarization despite heterocellular dye coupling and endothelial cell hyperpolarization in porcine ciliary artery. *J Vasc Res* **34**, 344–350.

Beyer EC, Gemel J, Seul KH, Larson DM, Banach K & Brink PR (2000). Modulation of intercellular communication by differential regulation and heteromeric mixing of co-expressed connexins. *Braz J Med Biol Res* **33**, 391–397.

Busse R, Edwards G, Feletou M, Fleming I, Vanhoutte PM & Weston AH (2002). EDHF: bringing the concepts together. *Trends Pharmacol Sci* **23**, 374–380.

Ceelen PW, Lockridge A & Newman EA (2001). Electrical coupling between glial cells in the rat retina. *Glia* **35**, 1–13.

Chen G, Hashitani H & Suzuki H (1989). Endothelium-dependent relaxation and hyperpolarization of canine coronary artery smooth muscles in relation to the electrogenic Na-K pump. *Br J Pharmacol* **98**, 950–956.

Coleman HA, Tare M & Parkington HC (2001*a*). EDHF is not K^+ but may be due to spread of current from the endothelium in guinea pig arterioles. *Am J Physiol Heart Circ Physiol* **280**, H2478–H2483.

Coleman HA, Tare M & Parkington HC (2001*b*). K^+ currents underlying the action of endothelium-derived hyperpolarizing factor in guinea-pig, rat and human blood vessels. *J Physiol* **531**, 359–373.

Doughty JM, Boyle JP & Langton PD (2000). Potassium does not mimic EDHF in rat mesenteric arteries. *Br J Pharmacol* **130**, 1174–1182.

Edwards G, Dora KA, Gardener MJ, Garland CJ & Weston AH (1998). K^+ is an endothelium-derived hyperpolarizing factor in rat arteries. *Nature* **396**, 269–272.

Edwards GM, Feletou M, Gardener MJ, Thollon C, Vanhoutte PM & Weston AH (1999*b*). Role of gap junctions in the responses to EDHF in rat and guinea-pig small arteries. *Br J Pharmacol* **128**, 1788–1794.

Edwards G, Gardener MJ, Feletou M, Brady G, Vanhoutte PM & Weston AH (1999*a*). Further investigation of endothelium-derived hyperpolarizing factor (EDHF) in rat hepatic artery: studies using 1-EBIO and ouabain. *Br J Pharmacol* **128**, 1064–1070.

Emerson GG & Segal SS (2000). Electrical coupling between endothelial cells and smooth muscle cells in hamster feed arteries: role in vasomotor control. *Circ Res* **87**, 474–479.

Faraci FM & Heistad DD (1998). Regulation of the cerebral circulation: role of endothelium and potassium channels. *Physiol Rev* **78**, 53–97.

Feletou M & Vanhoutte PM (1988). Endothelium-dependent hyperpolarization of canine coronary smooth muscle. *Br J Pharmacol* **93**, 515–524.

Feletou M & Vanhoutte PM (1999). The alternative: EDHF. *J Mol Cell Cardiol* **31**, 15–22.

Hashitani H, Windle A & Suzuki H (1998). Neuroeffector transmission in arterioles of the guinea-pig choroid. *J Physiol* **510**, 209–223.

Hille B (2001). *Ionic Channels of Excitable Membranes*. Sinauer Associates Inc, Sunderland, MA, USA.

Hirst GD, Choate JK, Cousins HM, Edwards FR & Klemm MF (1996). Transmission by post-ganglionic axons of the autonomic nervous system: the importance of the specialized neuroeffector junction. *Neuroscience* **73**, 7–23.

Hultcrantz E (1988). Clinical treatment of vascular inner ear diseases. *Am J Otolaryngol* **9**, 317–322.

Imaeda K, Yamamoto Y, Fukuta H, Koshita M & Suzuki H (2000). Hyperpolarization-induced dilatation of submucosal arterioles in the guinea-pig ileum. *Br J Pharmacol* **131**, 1121–1128.

Inoue T & Kannan MS (1988). Nonadrenergic and noncholinergic excitatory neurotransmission in rat intrapulmonary artery. *Am J Physiol* **254**, H1142–H1148.

Jiang F & Dusting GJ (2001). Endothelium-dependent vasorelaxation independent of nitric oxide and K^+ release in isolated renal arteries of rats. *Br J Pharmacol* **132**, 1558–1564.

Jiang ZG, Qiu JH, Ren TY & Nuttall AL (1999). Membrane properties and the excitatory junction potentials in smooth muscle cells of cochlea spiral modiolar artery in guinea pigs. *Hear Res* **138**, 171–180.

Jiang ZG, Si JQ, Lasarev MR & Nuttall AL (2001*a*). Two resting potential levels regulated by inward rectifying potassium channels in guinea pig cochlea spiral modiolar artery. *J Physiol* **537**, 829–842.

Jiang ZG, Si JQ & Nuttall AL (2001*b*). Acetylcholine induces hyperpolarization by opening calcium-activated K^+ channels via a NO-independent mechanism in guinea pig spiral modiolar artery. *Assoc Res Otolaryngol Midwin Res Meet Abstract* **24**, 29–30.

Jiang ZG, Zhao H, Dai CF & Nuttall AL (2003). Multi-mechanisms mediate acetylcholine-induced hyperpolarization and relaxation in smooth muscle cells of the spiral modiolar artery. *Assoc Res Otolaryngol Midwint Res Meet Abstract* **26**, 18.

Jiang ZG, Zhao H & Yang YQ (2004). Distinct channels responsible for acetylcholine-induced hyperpolarization and depolarization in guinea pig in vitro spiral modiolar artery. *Assoc Res Otolaryngol Midwint Res Meet Abstract* **27**, 996.

Lacy PS, Pilkington G, Hanvesakul R, Fish HJ, Boyle JP & Thurston H (2000). Evidence against potassium as an endothelium-derived hyperpolarizing factor in rat mesenteric small arteries. *Br J Pharmacol* **129**, 605–611.

Little TL, Xia J & Duling BR (1995). Dye tracers define differential endothelial and smooth muscle coupling patterns within the arteriolar wall. *Circ Res* **76**, 498–504.

Martin PE, Hill NS, Kristensen B, Errington RJ & Griffith TM (2003). Ouabain exerts biphasic effects on connexin functionality and expression in vascular smooth muscle cells. *Br J Pharmacol* **140**, 1261–1271.

McIntyre CA, Buckley CH, Jones GC, Sandeep TC, Andrews RC, Elliott AI, Gray GA, Williams BC, McKnight JA, Walker BR & Hadoke PW (2001). Endothelium-derived hyperpolarizing factor and potassium use different mechanisms to induce relaxation of human subcutaneous resistance arteries. *Br J Pharmacol* **133**, 902–908.

Miao FJ & Lee TJ (1991). VIP-ergic and cholinergic innervations in internal carotid arteries of the cat and rat. *J Cardiovasc Pharmacol* **18**, 369–378.

Neild TO, Shen KZ & Surprenant A (1990). Vasodilatation of arterioles by acetylcholine released from single neurones in the guinea-pig submucosal plexus. *J Physiol* **420**, 247–265.

Nilius B & Droogmans G (2001). Ion channels and their functional role in vascular endothelium. *Physiol Rev* **81**, 1415–1459.

Nuttall AL (1999). Sound-induced cochlear ischemia/hypoxia as a mechanism of hearing loss. *Noise Health* **5**, 17–31.

Quayle JM, Nelson MT & Standen NB (1997). ATP-sensitive and inwardly rectifying potassium channels in smooth muscle. *Physiol Rev* **77**, 1165–1232.

Quignard JF, Feletou M, Thollon C, Vilaine JP, Duhault J & Vanhoutte PM (1999). Potassium ions and endothelium-derived hyperpolarizing factor in guinea- pig carotid and porcine coronary arteries. *Br J Pharmacol* **127**, 27–34.

Schuknecht HF & Gacek MR (1993). Cochlear pathology in presbycusis. *Ann Otol Rhinol Laryngol* **102**, 1–16.

Si JQ, Zhao H, Yang YQ, Jiang ZG & Nuttall AL (2002). Nitric oxide induces hyperpolarization by opening ATP-sensitive K^+ channels in guinea pig spiral modiolar artery. *Hear Res* **171**, 167–176.

Spray DC & Bennett MV (1985). Physiology and pharmacology of gap junctions. *Annu Rev Physiol* **47**, 281–303.

Suga F & Snow JB Jr (1969). Cholinergic control of cochlear blood flow. *Ann Otol Rhinol Laryngol* **78**, 1081–1090.

Suzuki H (1988). The electrogenic Na-K pump does not contribute to endothelium-dependent hyperpolarization in the rabbit ear artery. *Eur J Pharmacol* **156**, 295–297.

Toda N, Ayajiki K & Okamura T (1997). Inhibition of nitroxidergic nerve function by neurogenic acetylcholine in monkey cerebral arteries. *J Physiol* **498**, 453–461.

Van Renterghem C, Vigne P & Frelin C (1995). A charybdotoxin-sensitive, Ca^{2+}-activated K^+ channel with inward rectifying properties in brain microvascular endothelial cells: properties and activation by endothelins. *J Neurochem* **65**, 1274–1281.

Weidelt T, Boldt W & Markwardt F (1997). Acetylcholine-induced K^+ currents in smooth muscle cells of intact rat small arteries. *J Physiol* **500**, 617–630.

Welsh DG & Segal SS (1997). Coactivation of resistance vessels and muscle fibers with acetylcholine release from motor nerves. *Am J Physiol* **273**, H156–H163.

Yamamoto Y, Klemm MF, Edwards FR & Suzuki H (2001). Intercellular electrical communication among smooth muscle and endothelial cells in guinea-pig mesenteric arterioles. *J Physiol* **535**, 181–195.

Yuan XJ, Tod ML, Rubin LJ & Blaustein MP (1995). Inhibition of cytochrome P-450 reduces voltage-gated K^+ currents in pulmonary arterial myocytes. *Am J Physiol* **268**, C259–C270.

Zhao H, Si JQ, Jiang ZG & Nuttall AL (2002). Different membrane and vasomotion properties between the spiral modiolar artery and the mesenteric artery in guinea pigs. *Assoc Res Otolaryngol Midwint Res Meet Abstract* **25**, 80.

Acknowledgements

This work was supported by grants from Deafness Research Foundation, Oregon Medical Research Foundation and NIH (NIDCD DC004716)(all to Z.-G.J.) and by NIH (NIDCD DC00105) and VA RR & D (RCTR 597–0160) (to A.L.N.). The authors are grateful for help with the statistics from Dr Gang Zheng (Office of Biostatistics Research, National Heart, Lung and Blood Institute, NIH) and for a reading of the manuscript by Dr Scott Matthews.

Supplemental material

The online version of this paper can be accessed at:
DOI:10.1113/jphysiol.2004.080960
http://jp.physoc.org/cgi/content/full/jphysiol.2004.080960/DC1
and contains supplemental material consisting of a table and five figures.
This material can also be found at:
http://www.blackwellpublishing.com/products/journals/suppmat/tjp/tjp822/tjp822sm.htm